metals

MDPI

Article

Effect of Temperature and Strain on Bonding of Similar AA3105 Aluminum Alloys by the Roll Bonding Process

Mauro Carta [1,*], Pasquale Buonadonna [1], Barbara Reggiani [2], Lorenzo Donati [3], Francesco Aymerich [1] and Mohamad El Mehtedi [1,*]

[1] Department of Mechanical, Chemical and Materials Engineering, University of Cagliari, 09123 Cagliari, Italy; pasquale.buonadonna@unica.it (P.B.); francesco.aymerich@unica.it (F.A.)
[2] DISMI Department of Sciences and Methods for Engineering, University of Modena and Reggio Emilia, Via Amendola 2, 42122 Reggio Emilia, Italy; barbara.reggiani@unimore.it
[3] DIN Department of Industrial Engineering, University of Bologna, Viale Risorgimento 2, 40136 Bologna, Italy; l.donati@unibo.it
* Correspondence: mauro.carta94@unica.it (M.C.); m.elmehtedi@unica.it (M.E.M.)

Abstract: Accumulative roll bonding (ARB) is a severe plastic deformation process that enables the production of materials with ultrafine microstructures and enhances the characteristics of the base material, particularly in metal matrix composites. The primary objective of this study is to experimentally investigate the bonding strength in AA3105 strips that underwent the roll bonding process, with a specific focus on examining the influence of temperature and reduction rate on bonding. Three temperature levels (200 °C, 300 °C, and 400 °C) and three thickness reduction levels (35%, 50%, and 65%) were considered. The T-peel test was carried out to assess the bonding quality. It was employed to determine the peak force required to separate the two bonded strips. Additionally, ANOVA analysis was performed to develop a regression equation for analyzing peak force. Optical microscopy was used to evaluate the interface bonding quality in the longitudinal section. The results indicate that the bonding strength increases with both temperature and percentage reduction.

Keywords: aluminum; accumulative roll bonding; AA3105; T-peel test; design of experiment; ANOVA

Citation: Carta, M.; Buonadonna, P.; Reggiani, B.; Donati, L.; Aymerich, F.; El Mehtedi, M. Effect of Temperature and Strain on Bonding of Similar AA3105 Aluminum Alloys by the Roll Bonding Process. *Metals* **2024**, *14*, 920. https://doi.org/10.3390/met14080920

Academic Editor: Tianliang Fu

Received: 15 July 2024
Revised: 8 August 2024
Accepted: 10 August 2024
Published: 14 August 2024

1. Introduction

The research for new materials with characteristics of lightness and excellent mechanical properties has been increasing in recent decades. Among the most promising technological processes is accumulative roll bonding, a key method within the array of severe plastic deformation (SPD) processes. These include techniques like friction stir processing (FSP) and equal-channel angular pressing (ECAP) [1], which allow beneficial mechanical properties to be obtained with respect to the base material. Even from an industrial point of view, it is the most promising SPD, scalable to large production, and is a continuous process [2,3].

The ARB process was first presented in 1998 by Saito et al. [4]. In this process, two initially separate sheets are coupled, usually with rivets, and hot or cold rolled together, and these steps are then repeated cyclically (Figure 1). To improve the bonding in the interface, the surfaces in contact must be brushed and polished with acetone. An annealing heat treatment could be processed after ARB to improve formability [5,6]. The ARB process was recently used to recycle aluminum chips [7].

The two strips could be similar or dissimilar materials to obtain different mechanical, electrical, chemical, thermal, etc., properties. One of the first works joining different materials was by Izadju et al. [8], who studied the effects on mechanical properties in Al/Cu composites.

It is also possible to produce metal matrix composites (MMCs) with the ARB process by placing particles between the strips. Alizadeh and Paydar [9] studied the effects of

SiC particles on the effect of mechanical properties, while Rezayat and Akbarzadeh [10] investigated the effect of alumina particles with pure aluminum sheets.

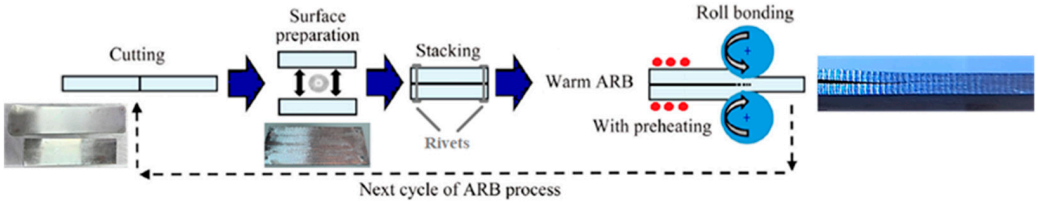

Figure 1. Schematic diagram of the ARB process [3].

Several studies have been carried out on the mechanism of bond formation that is generated because of the ARB process. Film theory is one of the most accredited for cold bonding and asserts that a bond is formed between two surfaces if these are properly treated, clean, and in close contact, under conditions of optimal temperature and rolling pressure [11]. Under these conditions, the surface layers crack and the underlying materials are extruded together. The hot ARB bonding process, instead, is more related to diffusion bonding and recrystallization theory.

Bonding strength is essential to ensure excellent mechanical properties after the ARB process. The T-peel test is a test developed to evaluate the peeling force required to separate adhesives. It was successfully applied by Quadir et al. [12] to evaluate the toughness of the bonding on commercial-purity aluminum strips, and successively applied by other authors [13]. Lu et al. [14] demonstrated that the addition of SiO2 particles in the bonding interface of AA6060 increases the bond strength after the ARB process. Samadzadeh et al. [15] studied the influence of reduction and MWCNT particles on the bonding strength with the usage of the T-peel test. Particularly in cold-roll bonding, the usage of particles can enhance the bonding strength [16]. Various authors studied the influence of particles in bonding [17,18] and also in the bonding of different materials [19].

El Mehtedi et al. [3] studied the effect of the ARB process on the AA3105 aluminum alloy until the fourth cycle. The experiments were carried out at 300 °C and 50% reduction, with a maximum increment of UTS at the third ARB cycle of 235 MPa, 53% higher than the annealed condition. Examination of the tensile fracture surface revealed that debonding consistently occurred at the interface formed during the last pass, indicating insufficient strength at this juncture. Other authors studied the ARB process on Al-Mn alloys; for example, Xing et al. [20] investigated how varying the number of ARB cycles impacts grain refinement and strengthening in Al-3003 alloy processed at 250 °C. They found similar results in their work, finding that deboning always occurs in the last ARB interface (reduction of 50%), while the interface layer of the precious ARB cycles completely disappears (reduction higher than 75%). Chowdhury et al. [21] studied the effect of the ARB process on the texture evolution of AA3103, finding that the pole figures are symmetric during the process up to five cycles. The need to improve adhesion strength appeared evident. Delshad Gholami et al. [22] studied the effect of temperature on the mechanical properties and forming diagram of pure commercial aluminum, and, additionally, they found that elevated temperatures facilitate stronger bonding between the layers.

This study aimed to evaluate the bonding strength between the surfaces of two AA3105 strips after one cycle of the roll bonding process. The focus is on the force required to separate the original strips, assessed using the T-peel test. The ARB process involves numerous parameters that influence the quality of the outcome. In this study, experiments were conducted at various temperatures and reductions to identify the optimal bonding conditions. The surface sections of the strips were examined using optical micrography with polarized light. Surface response analysis in Minitab was then used to analyze the bonding strength, leading to the proposal of a regression equation.

2. Materials and Methods

The chemical composition of AA3105, which was used in this study, is provided in Table 1. The material was initially supplied as a 6 mm thick sheet, manufactured through twin roll casting. It was subsequently hot rolled at 400 °C to achieve a thickness of 2.8 mm, followed by two cold-rolling steps to reduce the thickness to 1.2 mm. The sheets were then annealed for a total of 4 h in an electric muffle furnace at 400 °C, and air cooled to room temperature.

Table 1. Chemical composition of AA3105 alloy (wt.%).

Elements	Si	Fe	Cu	Mn	Mg	Cr	Zn	Ti	Al
Contents	0.23	0.45	0.11	0.51	0.70	0.006	0.01	0.05	Balanced

The sheets were cut into dimensions of 90 × 30 × 1.2 mm^3, and 3 mm diameter through-holes were drilled at both ends using a column drill for riveting. Then, mechanical surface roughening was performed using an orbital brusher with 80-grit abrasive discs, followed by cleaning with acetone. Chalk powder was applied to prevent bonding on one side of the samples for a length of approximately 20 mm. This step is necessary for the T-peel test described thereafter.

To investigate the effects of rolling reduction and temperature on the samples, a full factorial design of experiment (DoE) was carried out with two factors and three levels each (Table 2). The samples underwent a single pass of accumulative roll bonding (ARB), also known as the roll bonding (RB) process, with three levels of thickness reduction: 35%, 50%, and 65%. This was done at varying rolling temperatures of 200 °C, 300 °C, and 400 °C for a total of 9 different conditions. Before rolling, each specimen was heated in the furnace for 10 min at the deformation temperature. The time taken to transfer the specimens from the furnace to the rolling mill was approximately 2 s. The rolling process was performed along the original rolling direction of the specimens.

Table 2. DoE full factorial design summary table.

Factors			Levels		
Name	**Units**	**Symbols**	**1**	**2**	**3**
Temperature	[°C]	T	200	300	400
Reduction	[%]	r	35	50	65

The rolling process was carried out using a duo high-rolling mill (BW200, Carl Wezel, Mühlacker, Germany); the rollers' diameter is 130 mm and the rotation speed is 52 rpm. The mean thickness of the specimens after the roll bonding process was measured and is presented in Table 3. Notably, the thickness exhibited minor variations based on the rolling temperature, even though the same machine configuration was used.

Table 3. Theoretical thickness after the roll bonding process, and actual mean thickness measured on the specimens.

Theoretical Reduction	T = 200 °C Mean Thickness [mm]	T = 300 °C Mean Thickness [mm]	T = 400 °C Mean Thickness [mm]
35% (1.56 mm)	1.50	1.51	1.56
50% (1.20 mm)	1.17	1.17	1.22
65% (0.84 mm)	0.90	0.94	0.96

Subsequently, the bonding-free zone of each specimen was bent to form a 90° angle relative to the rolling direction, as illustrated in Figure 2a. This bending is essential to create a gripping zone for the peel test, ensuring a secure grip.

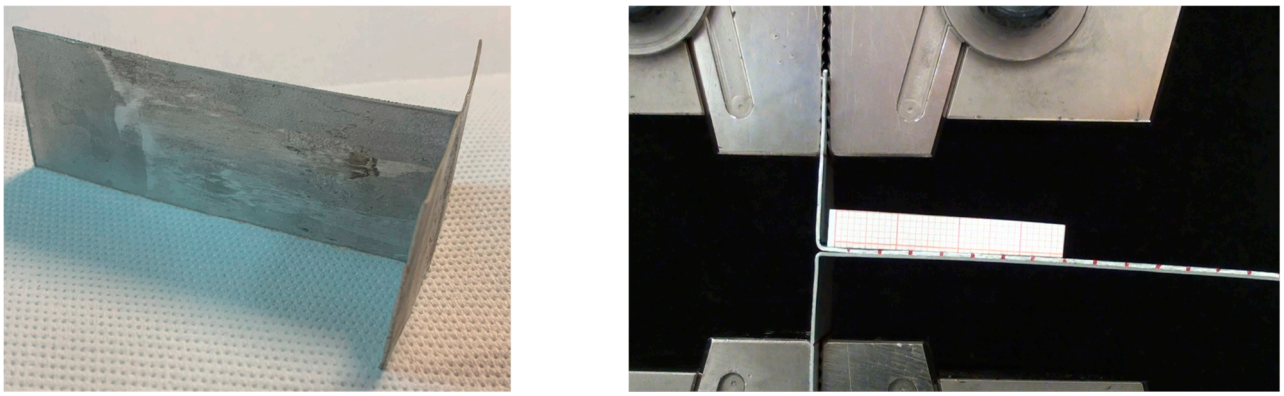

(**a**) (**b**)

Figure 2. (**a**) Specimen with the two sheets bent to 90° in order to perform the T-peel test; (**b**) T-RB sample during the T-peel test.

All the specimens were tested using a Galdabini Sun 500 material testing machine (Figure 2b), with the machine gripping the tabs to evaluate the specimens' behavior during the destructive bonding test and to analyze the failure mode according to ASTM D1876 [23]. Three specimens were tested under each set of conditions.

In order to observe the bonding section, micrography was conducted under polarized light using a Leica Z8 Wild M420 optical microscope equipped with a Canon EOS 650D for every test condition. The experiments were conducted in the Laboratory of Manufacturing Systems at the University of Cagliari. The samples were cut along the rolling direction (RD) and the surface was polished with electrochemical polishing in a 75% phosphoric acid solution at 75 °C and etched with an HBF_4 acid solution at 5%. The results obtained from these tests are discussed below.

3. Results and Discussion

3.1. Peeling Test Results

The bonding behavior varied with increasing rolling temperature and percentage reduction, resulting in different opening modes. The samples with inferior bonding interfaces exhibited a rupture mode that caused elastic deformation of the sheets affected by the adhesive interface (as shown in Figure 3a). Conversely, high temperatures and significant percentage reductions resulted in greater bonding strength, with plastic deformation of the coupled sheets after the test. Figure 3b shows a sample with a slight curve away from the zone of separation, suggesting some degree of plastic deformation. Figure 3c depicts a sample with a significant amount of bending and twisting along the separation line, which implies a more ductile behavior and a stronger bond that has undergone plastic deformation before failing.

At higher rolling temperatures, materials tend to be more ductile and exhibit greater deformation under the same applied load compared to lower temperatures. The flow stress of the alloy changes with temperature. At higher temperatures, it has lower flow stress, and so it is easier to deform, with lower deformation of the rolls. The different thicknesses of the samples shown in Table 3 can affect their response to the peel test. Different thicknesses result in different sections of the samples during the test, leading to different modes of failure (e.g., cohesive failure within the material or adhesive failure at the interface). The force–displacement curve obtained during the peel test may exhibit different characteristics depending on the material's ductility and deformation behavior, ultimately affecting the interpretation of the test results. The peak force, however, should not be affected by the thickness variation, but only by the bonding strength; this is why it is taken into account in the following.

The force and displacement data from the T-peel test are presented in Figure 4, with the force normalized by the bonding width. At 200 °C with a 35% or 50% reduction, the

peel force is notably low, and there is a minimal difference between the initial peak force and the force required for crack propagation. The peak force increases at 200 °C with a 65% reduction, but diminishes rapidly after a slight displacement, indicating that once the crack starts, it propagates easily, leading to the separation of the strips at the interface layers. At 300 °C, a 35% reduction results in weak bonding, whereas at 50% and 65% reductions, the difference between the peak force and the steady force for crack propagation is small and remains high even after the crack initiates.

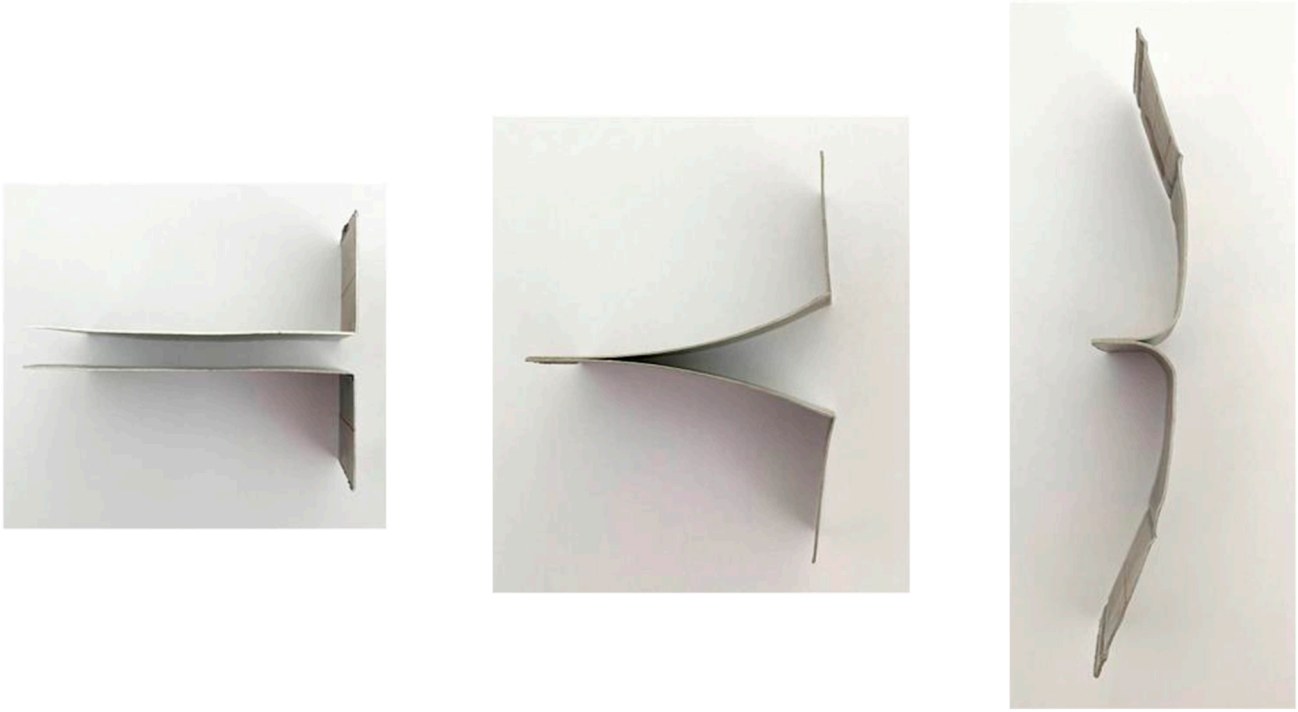

(**a**) (**b**) (**c**)

Figure 3. T-peel specimens after testing with different deformation modes: (**a**) sample with elastic deformation indicating inferior bonding; (**b**) slight plastic deformation with moderate bonding strength; (**c**) significant plastic deformation and ductile behavior suggesting a strong bond between strips.

At 400 °C, the bonding is excellent across all levels of reduction, with the samples at 50% and 65% reduction being particularly resistant to opening at the interface layer due to high plastic deformation, indicating very strong bonding.

Figure 5 displays the diagram of the peak force required to initiate crack formation at the interface layer, further confirming the exceptional bonding quality at 400 °C for all analyzed reductions. The bonding at 300 °C and 65% reduction is excellent, and it remains good at 300 °C with 50% reduction. The chart shows a consistent pattern where the force increases with temperature and reduction percentage.

According to the Plata–Piwnik criterion [24], the bonding in the solid-state process of aluminum is expressed as follows:

$$w = \int_0^t \frac{p}{\sigma_{eff}} dt \geq w_{lim} \quad \text{where} \quad w_{lim} = 4.9063e^{-0.0017T} \tag{1}$$

Here, p represents the normal contact pressure, σ_{eff} represents the effective stress, and T is the temperature in °C. According to this criterion, bonding occurs when the value of w exceeds w_{lim}. This limit is temperature-dependent, with higher temperatures resulting in lower limits. Thus, it becomes clear why good bonding is achieved at higher temperatures in every reduction condition (Figure 5).

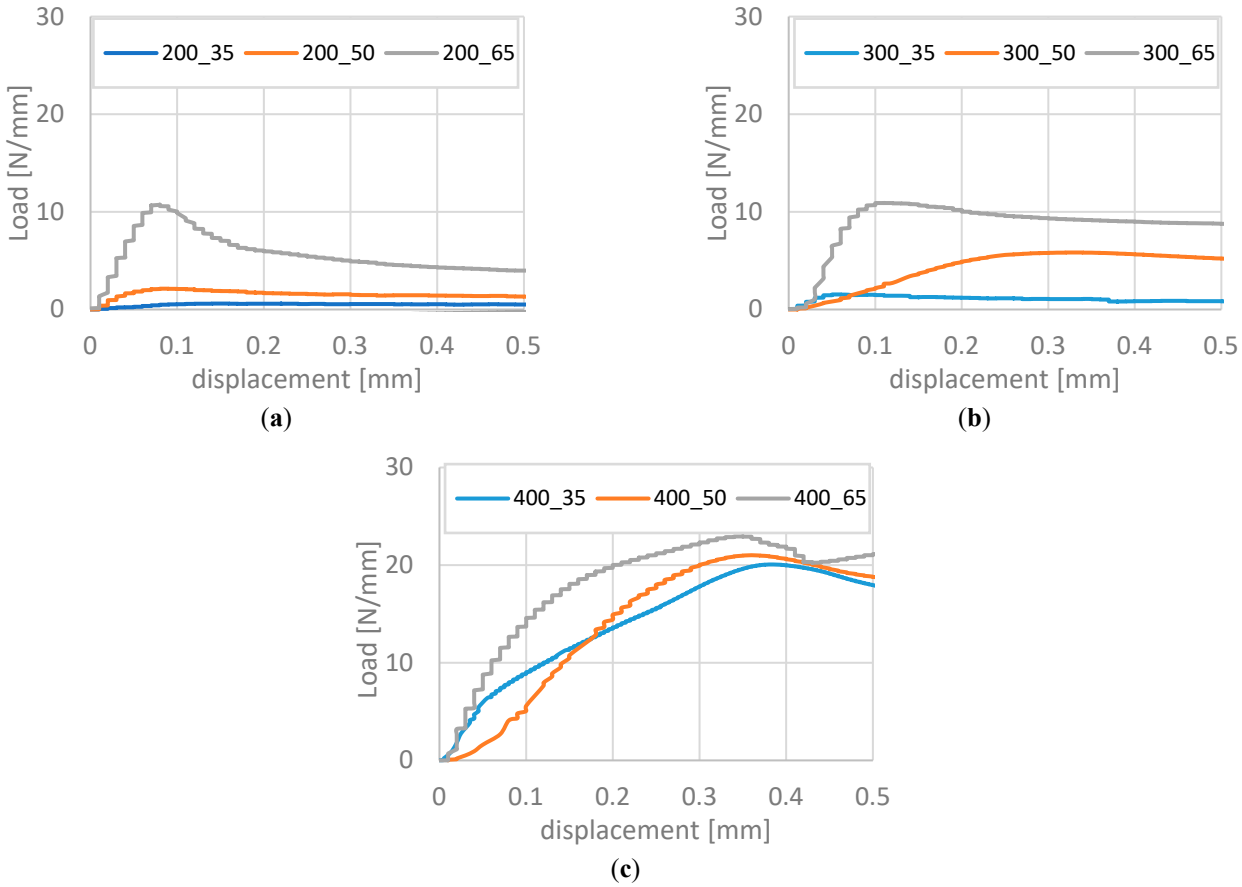

Figure 4. Examples of load normalized width vs. displacement of the T-peel tests for every condition: (**a**) 200 °C (**b**) 300 °C; (**c**) 400 °C.

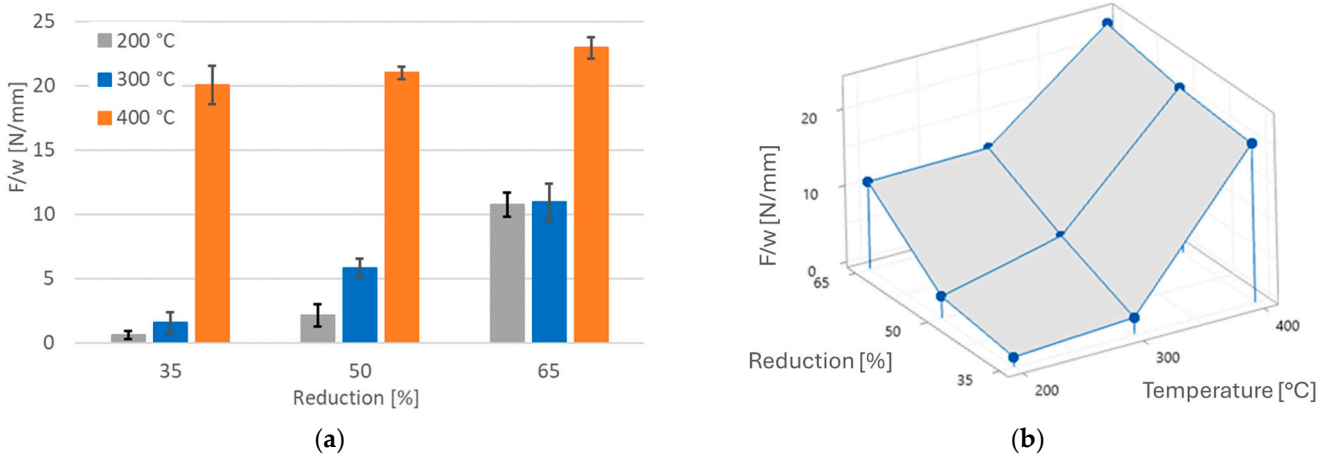

Figure 5. Different representations of experimental data: (**a**) diagram of F/w and (**b**) 3D representation of F/w as a function of temperature and reduction rate.

The data shown in Figure 5 are consistent with the different opening behaviors shown in Figure 3. Specifically, the higher the peak force, greater the chance of experiencing plastic deformation during the T-peel test (Figure 3b,c). Conversely, if the opening force during the test is low, the sample may respond with only elastic deformation (Figure 3a). The configuration at 200 °C and 35% and 50% showed an opening behavior similar to Figure 3a, with only elastic deformation. At 300 °C and 50% reduction, the opening behavior is the

same as that in Figure 3b, while at 400 °C, in every condition, the opening behavior aligns with Figure 3c. These results indicate that the higher the peel force, the greater the chance of experiencing plastic deformation during the T-peel test, correlating with higher bonding strength. Conversely, if the opening force during the test is low, the sample may only undergo elastic deformation, resulting in a lower bonding strength.

3.2. Response Surface Analysis

Experimental results were elaborated in Minitab v.19 software. Surface response analysis was applied to the data with a central composite design, resulting in a model with an R^2 value of 98.8% and an adjusted R-squared (Radj2) of 97%. Table 4 presents the analysis of variance, indicating that T (in °C), r (in %), and T^2 terms are statistically significant in the process, based on the *p*-value and a significance level set at 0.05.

Table 4. Analysis of variance for the model.

Analysis of Variance					
Terms	**DF**	**Adj SS**	**Adj MS**	**F-Value**	***p*-Value**
Linear Terms					
Temperature	1	425.564	425.564	181.67	0.001
Reduction	1	83.579	83.579	35.68	0.009
Square Terms					
Temperature^2	1	92.981	92.981	39.69	0.008
Reduction^2	1	4.365	4.365	1.86	0.266
2-Way Interaction					
Temperature × reduction	1	13.092	13.092	5.59	0.099

It is commonly held in statistical analysis that regressors with a *p*-value greater than 0.05 do not pass the significance threshold in a hypothesis test, indicating their impact on the response variable may not be significant. Notably, research suggests that at a *p*-value of exactly 0.05, there is a substantial risk—potentially up to 50%—of incorrectly rejecting a true null hypothesis [25]. This risk increases as the *p*-value approaches this cutoff from below. Given this understanding, the variables temperature (T), reduction (r), and the square of temperature (T^2) can be considered statistically significant contributors to the model, as their associated *p*-values are well below the 0.05 threshold.

A subsequent analysis, applying surface response methodology to the dataset using only the significant parameters, yielded a model with an R^2 of 96.09% and an adjusted R-squared ($Radj^2$) of 93.75%. Table 5, which includes the ANOVA, reaffirms the statistical significance of T, r, and T^2 in the process, supporting the conclusions drawn from the initial analysis of variance.

Table 5. Analysis of variance for the second model.

Analysis of Variance					
Terms	**DF**	**Adj SS**	**Adj MS**	**F-Value**	***p*-Value**
Linear terms					
Temperature	1	425.56	425.564	86.90	0.000
Reduction	1	83.58	83.579	17.07	0.009
Square Terms					
Temperature^2	1	92.98	92.981	18.99	0.007

The mathematical model describes the peak force per width (N/mm) as a function of temperature (T) in degrees Celsius and the reduction variable (r) as a percentage.

Equation (2) shows the complete regression equation obtained from the second model and represented in the 3D plot of Figure 6.

$$F/w = 29.8 - 0.3249 \cdot T + 0.2488 \cdot r + 0.000682 \cdot T^2 \quad (2)$$

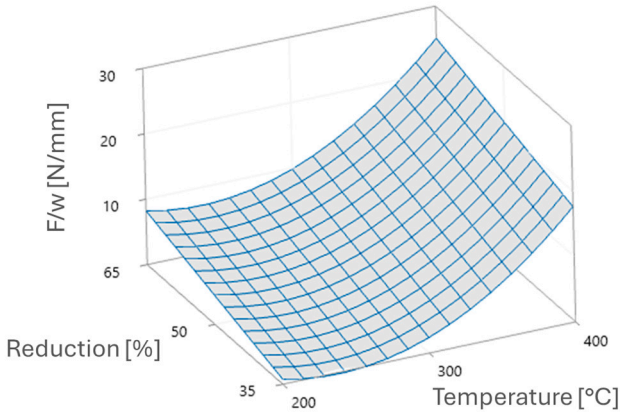

Figure 6. Surface plot for peak force per width as a function of temperature and reduction percentage.

According to the ANOVA analysis, the variables temperature (T), reduction (r), and the square of temperature (T^2) can be considered statistically significant contributors to the model. This can help understand the influence of these variables in the process, particularly on the peak force values. The lower the *p*-value, the higher the significance of these parameters on the outcome. Specifically, the order of significance, according to Table 5, is T, T^2, and r.

The model suggests a linear relationship with both T and r, as well as a quadratic relationship with T (indicated by the term T^2). The coefficients in the equation quantify the influence of each term. The three-dimensional plot visualizes how F/w varies with T and r.

The curvature of the surface on the plot suggests a complex relationship between T, r, and F/w, where F/w increases as T increases, but the rate of increase changes with different values of r. The graph is essential for visualizing the combined effect of T and r on F/w, which would not be as evident from the equation alone. Such a plot is typically used to predict the peak force for given levels of temperature and reduction (r). It serves as a tool for understanding the interplay between the variables and for optimizing the conditions to achieve a desired F/w value. The surface plot, together with the equation, provides a comprehensive visual and mathematical representation of the behavior of peak force as influenced by temperature and the variable r.

Figure 7 is a bar graph comparing predicted and experimental values for the F/w variable and can be useful to visually assess the accuracy of the predictive model against actual observed data.

The blue bars represent the predicted values of F/w using Equation (2), while the red bars show the experimental values. In general, the predicted values closely match the experimental values, suggesting that the model used for the predictions has good accuracy. For most conditions, the predicted values are slightly higher than the experimental values, which suggests that the model might systematically underestimate the F/w. In particular, a systematic deviation is observed in which the predictive model consistently overestimates the F/w values in six out of nine experimental conditions. Despite this, the predicted values are generally in close agreement with the experimental ones. The difference of the model with experimental results is in the range ± 2.5 N/mm. A calibration using a more robust dataset, with more samples, could improve its predictive power. Moreover, the model's current form may still provide valuable insights into the trend of F/w changes across conditions.

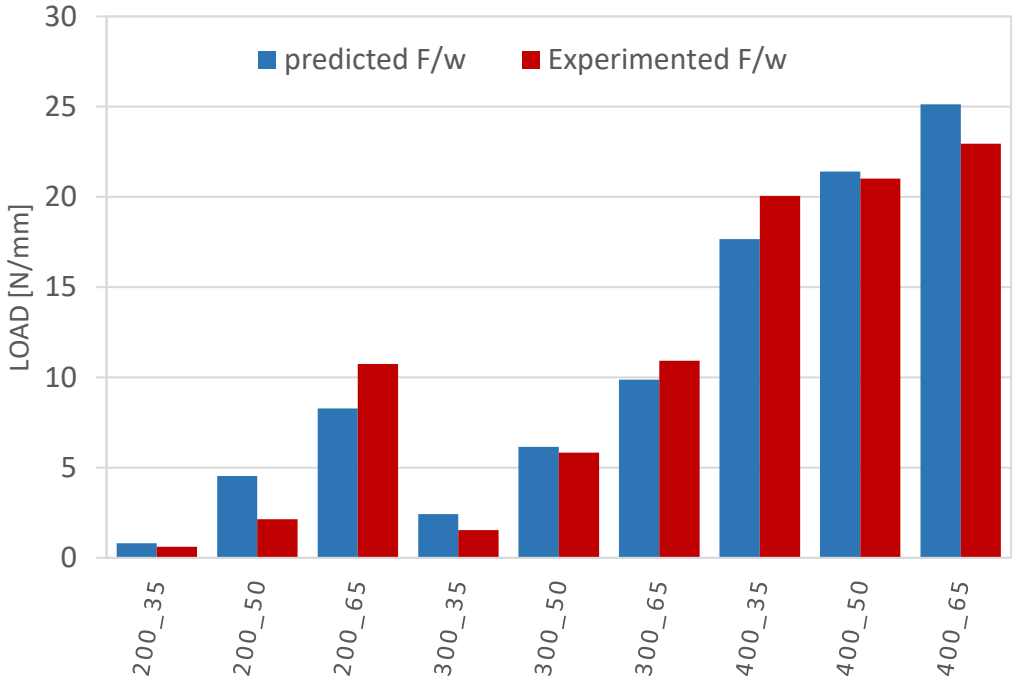

Figure 7. Comparison between experimental and predicted results.

3.3. Optical Micrograph of the Samples

The optical micrographs were carried out with the purpose of observing the interface bonding layer. Figure 8 shows samples treated at different temperatures and levels of reduction. According to Lee et al., well-bonded samples have an interface layer that is not easily discernible in ARB samples of aluminum alloys [26]. A well-bonded interface can be difficult to distinguish because of the effective diffusion of atoms across the boundary, leading to a more homogeneous microstructure. Therefore, the more difficult it is to distinguish the interface layer, the more likely it is that the bond between the strips is strong.

Figure 8a–c show micrographs of samples processed at 200 °C with reductions of (a) 35%, (b) 50%, and (c) 65%. The micrographs reveal the interface layers, marked by arrows. The interface layer in sample (c) is not easy to discern, in accordance with the T-peel test, where the bond strength was quite good. Figure 8d–f display micrographs of samples processed at the higher temperature of 300 °C. The samples exhibit different characteristics with increasing reductions. In particular, sample (f) at 65% reduction has a good interface layer, indicating a more successful bonding outcome, likely due to improved diffusion and adhesion at the elevated temperature. The interface layer is slightly visible at 400 °C and 35% reduction (Figure 8g), while it is almost impossible to distinguish at 50% and 65% reduction (Figure 8h,i). In summary, at 200 °C and 300 °C, interface bonding is observable at reductions of 35% and 50%, but not easily discernible at 65%. At 400 °C, it becomes increasingly challenging to detect the interface layer with each reduction.

AA3105 is not a heat-treatable alloy, and the increase in dislocation density contributes to the strengthening of the material through mechanisms such as strain hardening.

The specimen processed by one cycle of accumulative roll bonding (ARB) exhibits a microstructure characterized by relatively large grains that are elongated in the rolling direction. This alloy does not undergo dynamic recrystallization during deformation at high temperature due to the presence of manganese dispersoid of Al_6Mn, resulting in a fibrous microstructure caused by the high deformation undergone during the rolling process and visible at every rolling temperature and reduction (Figures 9–11).

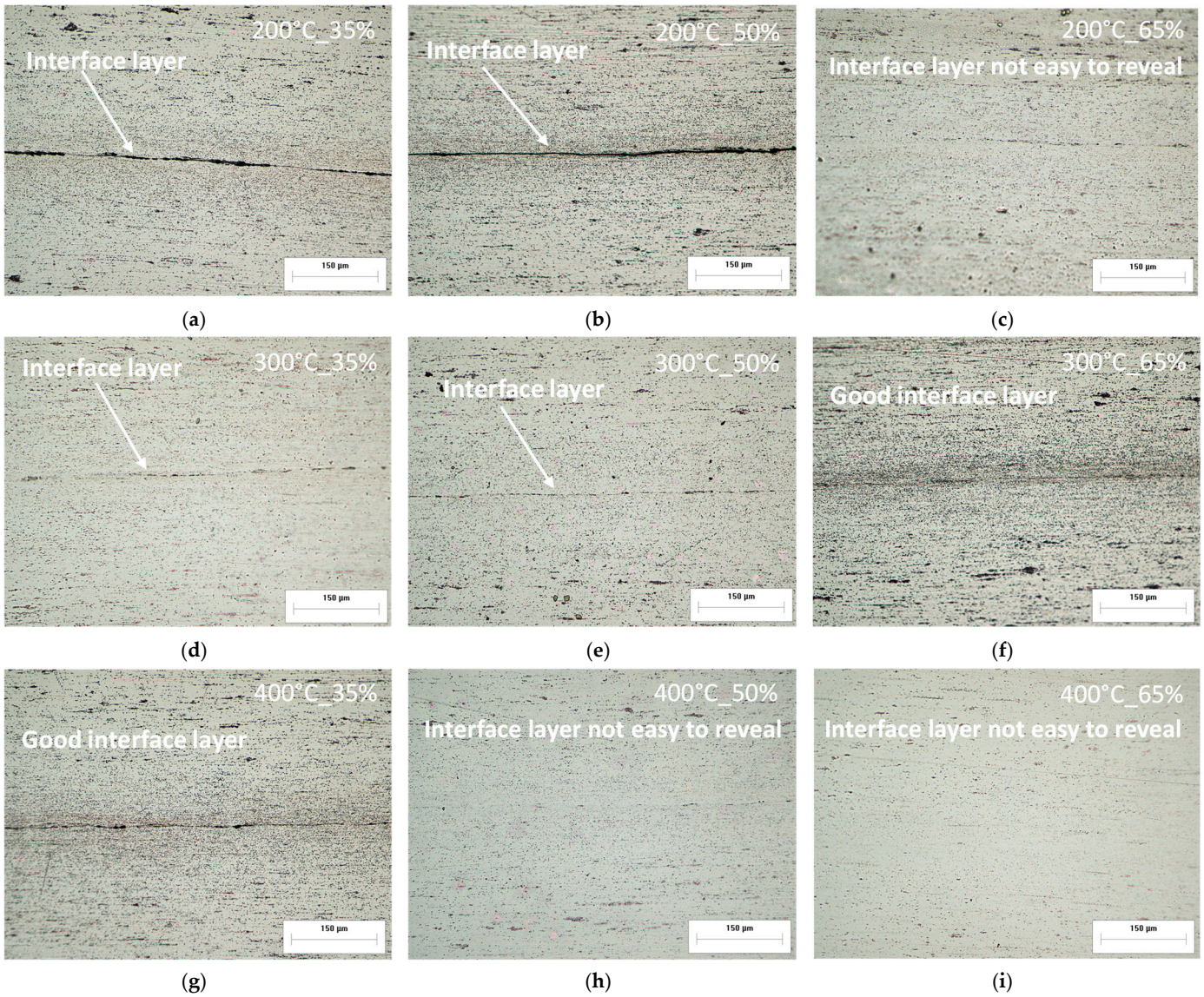

Figure 8. Micrographs by OM at 200 °C and reductions of (**a**) 35%, (**b**) 50%, and (**c**) 65%; at 300 °C and reductions of (**d**) 35%, (**e**) 50%, and (**f**) 65%; at 400 °C and reductions of (**g**) 35%, (**h**) 50%, and (**i**) 65%.

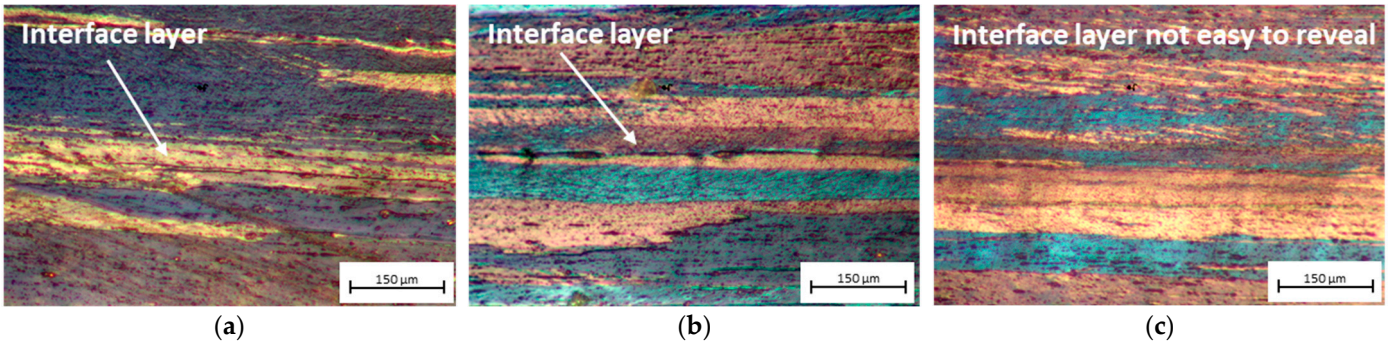

Figure 9. Micrographs by OM with polarized light at 200 °C and reductions of (**a**) 35%, (**b**) 50%, and (**c**) 65%.

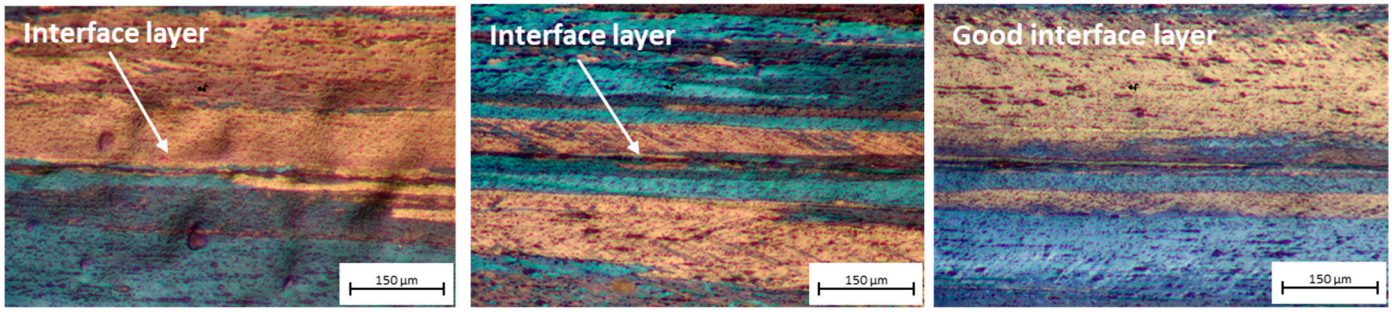

(**a**) (**b**) (**c**)

Figure 10. Micrographs by OM with polarized light at 300 °C and reductions of (**a**) 35%, (**b**) 50%, and (**c**) 65%.

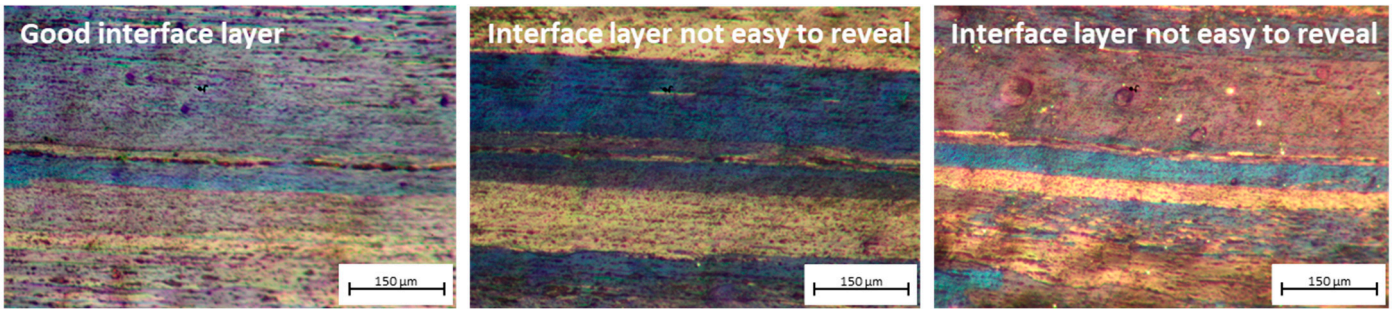

(**a**) (**b**) (**c**)

Figure 11. Micrographs by OM with polarized light at 400 °C and reductions of (**a**) 35%, (**b**) 50%, and (**c**) 65%.

The presence of Mn and Fe in the chemical composition leads to intermetallic formations. Figure 12 shows a SEM image of the sample hot rolled at 400 °C and 50%, and it suggests the presence of intermetallic formations that are rich in these two elements. The needle-like shape of the inclusions (in light grey in the image) indicates β-AlFeSi [27]. Some β-AlFeSi phase particles transform into α-Al(FeMn)Si, shown as small rounded intermetallic formations. A eutectic residual phase derived from the twin-roll cast production process of the alloy is still visible.

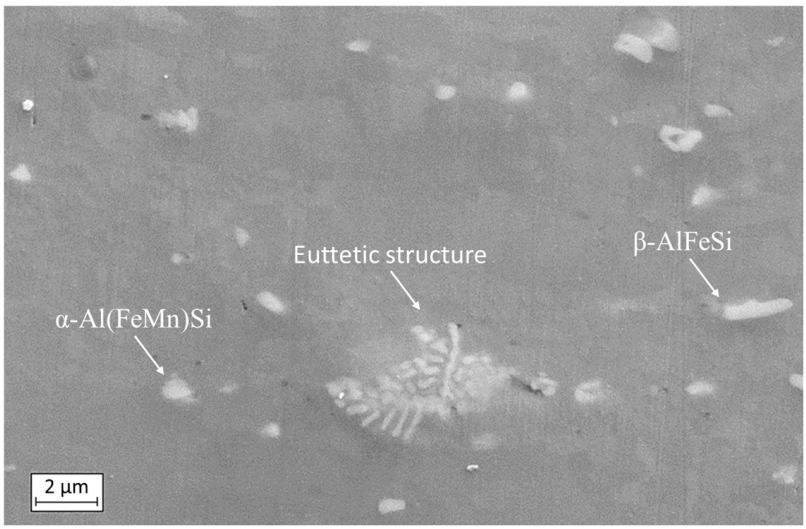

Figure 12. SEM image of 400 °C sample (50% reduction), 3000×.

The difficulty in discerning the interface layers at elevated temperatures and reductions suggests a transition toward a more homogenized structure. These findings align with the T-peel test results, which support the interpretation of improved bonding quality under such conditions. As the reduction and temperature increase, the interface layer becomes less distinct, indicating a stronger bond. This further corroborates that the bonding quality is significantly affected by rolling parameters, particularly temperature and percentage reduction. At higher values of these parameters, the interface layer becomes increasingly indistinct, reinforcing the relationship between processing conditions and bond integrity.

Our study identifies a clear trend of increasing bonding strength with higher temperatures and greater thickness reductions. However, it is crucial to consider that practical limits of these parameters exist for industrial applications, particularly regarding energy consumption and material oxidation. At 400 °C, peel test results indicate that the peak force is very similar across different reductions, suggesting that further increasing the temperature may not yield significant benefits. From an industrial perspective, it is essential to balance quality bonding with process efficiency and energy consumption. Higher temperatures and reductions demand more energy, which increases operational costs. Zinong et al. [28] found that at 580 °C and 60% deformation, the welding interfaces disappeared completely in pure aluminum, indicating excellent bonding. However, such a high temperature—nearing the melting point—may be inconvenient for industrial applications due to excessive energy requirements and potential material oxidation, which may not be suitable for some applications. Therefore, optimizing the process at lower temperatures would be beneficial for industrial applications, ensuring strong bonds while minimizing energy consumption and maintaining material integrity.

4. Conclusions

In this work, two aluminum strips of AA3105 aluminum alloy were roll bonded at a different temperature and different reduction rate. The conclusions are as follows:

- At 400 °C, the bonding properties were excellent across all levels of rolling reduction. Higher temperatures and reductions, in the studied range, resulted in a more uniform, homogenized material, indicating a stronger metallurgical bond.
- At 300 °C and 65% reduction, good bonding quality was observed, with no significant decrease in force after crack initiation during the peel tests. At 35% reduction, bonding was weak, while an intermediate condition was found at 50% reduction.
- At 200 °C, with 35% and 50% reduction, the quality of the bonding was poor, with minimal difference between the initial peak force and the force required for crack propagation. At 65% reduction, the peak force was quite high but showed a noticeable drop in force after the crack began to propagate, indicating inferior bonding quality at lower temperatures.
- A response surface analysis model was created, suggesting its effectiveness in predicting bond strength indicated as the width-normalized peak force required to initiate cracking in the interface layer of the peel tests.

Author Contributions: Conceptualization, M.E.M., M.C. and P.B.; methodology, M.E.M. and M.C.; software, B.R. and P.B.; validation, L.D., F.A. and M.E.M.; formal analysis, M.E.M., M.C. and P.B.; investigation, M.C., P.B. and F.A.; resources, M.C., M.E.M. and F.A.; data curation, L.D., P.B., M.C. and M.E.M.; writing—original draft preparation, M.C., B.R. and L.D.; writing—review and editing, M.C., M.E.M. and P.B.; visualization, M.E.M., B.R., L.D., M.C., P.B. and F.A.; supervision, M.E.M., P.B. and F.A.; project administration, M.E.M., F.A. and P.B. funding acquisition, M.E.M., L.D. and B.R. All authors have read and agreed to the published version of the manuscript.

Funding: This study is funded by the Italian Ministry of University and Research, PNRR, Mission 4, Component 2, Investment line 1.1—Call for tender No. 104 published on 2.2.2022 by the Italian Ministry of University and Research (MUR), funded by the European Union—NextGenerationEU–Project Title: "SCULPTROL—SCULPTuring by ROLling for multi-material bonding"—CUP:

F53D23001830006—Grant Assignment Decree No 961 adopted on 30 June 2023 by the Italian Ministry of Ministry of University and Research (MUR).

Data Availability Statement: The raw data supporting the conclusions of this article will be made available by the authors on request.

Conflicts of Interest: The authors declare no conflicts of interest.

References

1. Carta, M.; Buonadonna, P.; Marongiu, G.; Mehtedi, M.E. Analysis of Friction Stir Processed Surface Quality of AA2098 Aluminum Alloy for Aeronautical Applications. *Metall. Mater. Eng.* **2023**, *29*, 16–23. [CrossRef]
2. Ghalehbandi, S.M.; Malaki, M.; Gupta, M. Accumulative Roll Bonding—A Review. *Appl. Sci.* **2019**, *9*, 3627. [CrossRef]
3. El Mehtedi, M.; Lai, D.; Almehtedi, R.; Carta, M.; Buonadonna, P.; Aymerich, F. Bonding of similar AA3105 aluminum alloy by Accumulative Roll Bonding process. *ESAFORM 2021* **2021**, *942*, 1–11. [CrossRef]
4. Saito, Y.; Utsunomiya, H.; Tsuji, N.; Sakai, T. Novel Ultra-High Straining Process for Bulk Materials-Development of the Accumulative Roll-Bonding (ARB) Process. *Acta Mater.* **1999**, *47*, 579–583. [CrossRef]
5. Kwan, C.; Wang, Z. Microstructure Evolution upon Annealing of Accumulative Roll Bonding (ARB) 1100 Al Sheet Materials: Evolution of Interface Microstructures. *J. Mater. Sci.* **2008**, *43*, 5045–5051. [CrossRef]
6. Morovvati, M.R.; Dariani, B.M. The Effect of Annealing on the Formability of Aluminum 1200 after Accumulative Roll Bonding. *J. Manuf. Process.* **2017**, *30*, 241–254. [CrossRef]
7. El Mehtedi, M.; Buonadonna, P.; Carta, M.; El Mohtadi, R.; Mele, A.; Morea, D. Sustainability Study of a New Solid-State Aluminum Chips Recycling Process: A Life Cycle Assessment Approach. *Sustainability* **2023**, *15*, 11434. [CrossRef]
8. Eizadjou, M.; Kazemitalachi, A.; Daneshmanesh, H.; Shakurshahabi, H.; Janghorban, K. Investigation of Structure and Mechanical Properties of Multi-Layered Al/Cu Composite Produced by Accumulative Roll Bonding (ARB) Process. *Compos. Sci. Technol.* **2008**, *68*, 2003–2009. [CrossRef]
9. Alizadeh, M.; Paydar, M.H. Fabrication of Al/SiCP Composite Strips by Repeated Roll-Bonding (RRB) Process. *J. Alloys Compd.* **2009**, *477*, 811–816. [CrossRef]
10. Rezayat, M.; Akbarzadeh, A. Bonding Behavior of Al–Al2O3 Laminations during Roll Bonding Process. *Mater. Des. 1980–2015* **2012**, *36*, 874–879. [CrossRef]
11. Mori, K.; Bay, N.; Fratini, L.; Micari, F.; Tekkaya, A.E. Joining by Plastic Deformation. *CIRP Ann.* **2013**, *62*, 673–694. [CrossRef]
12. Quadir, M.Z.; Wolz, A.; Hoffman, M.; Ferry, M. Influence of Processing Parameters on the Bond Toughness of Roll-Bonded Aluminium Strip. *Scr. Mater.* **2008**, *58*, 959–962. [CrossRef]
13. Ruppert, M.; Böhm, W.; Nguyen, H.; Höppel, H.W.; Merklein, M.; Göken, M. Influence of Upscaling Accumulative Roll Bonding on the Homogeneity and Mechanical Properties of AA1050A. *J. Mater. Sci.* **2013**, *48*, 8377–8385. [CrossRef]
14. Lu, C.; Tieu, K.; Wexler, D. Significant Enhancement of Bond Strength in the Accumulative Roll Bonding Process Using Nano-Sized SiO2 Particles. *J. Mater. Process. Technol.* **2009**, *209*, 4830–4834. [CrossRef]
15. Samadzadeh, M.; Toroghinejad, M.R. The Influence of Carbon Nanotube and Roll Bonding Parameters on the Bond Strength of Al Sheets. *J. Mater. Eng. Perform.* **2014**, *23*, 1887–1895. [CrossRef]
16. Soltani, M.A.; Jamaati, R.; Toroghinejad, M.R. The Influence of TiO2 Nano-Particles on Bond Strength of Cold Roll Bonded Aluminum Strips. *Mater. Sci. Eng. A* **2012**, *550*, 367–374. [CrossRef]
17. Alizadeh, M. Effects of Temperature and B4C Content on the Bonding Properties of Roll-Bonded Aluminum Strips. *J. Mater. Sci.* **2012**, *47*, 4689–4695. [CrossRef]
18. Schmidt, C.W.; Knieke, C.; Maier, V.; Höppel, H.W.; Peukert, W.; Göken, M. Influence of Nanoparticle Reinforcement on the Mechanical Properties of Ultrafine-Grained Aluminium Produced by ARB. *Mater. Sci. Forum* **2010**, *667–669*, 725–730. [CrossRef]
19. Lee, K.S.; Bae, S.J.; Lee, H.W.; Kang, S.H. Interface-Correlated Bonding Properties for a Roll-Bonded Ti/Al 2-Ply Sheet. *Mater. Charact.* **2017**, *134*, 163–171. [CrossRef]
20. Xing, Z.P.; Kang, S.B.; Kim, H.W. Structure and Properties of AA3003 Alloy Produced by Accumulative Roll Bonding Process. *J. Mater. Sci.* **2002**, *37*, 717–722. [CrossRef]
21. Chowdhury, S.G.; Srivastava, V.C.; Ravikumar, B.; Soren, S. Evolution of Texture during Accumulative Roll Bonding (ARB) and Its Comparison with Normal Cold Rolled Aluminium–Manganese Alloy. *Scr. Mater.* **2006**, *54*, 1691–1696. [CrossRef]
22. Gholami, M.D.; Hashemi, R.; Sedighi, M. The Effect of Temperature on the Mechanical Properties and Forming Limit Diagram of Aluminum Strips Fabricated by Accumulative Roll Bonding Process. *J. Mater. Res. Technol.* **2020**, *9*, 1831–1846. [CrossRef]
23. D14 Committee ASTM International. Test Method for Peel Resistance of Adhesives (T-Peel Test). Available online: https://www.astm.org/d1876-08r15e01.html (accessed on 14 July 2024). [CrossRef]
24. Plata, M.; Piwnik, J. Theoretical and Experimental Analysis of Seam Weld Formation in Hot Extrusion of Aluminum Alloys. *Proc. 7th Int. Alum. Extrus. Technol. Semin.* **2000**, *1*, 205–211.
25. Tronci, A.; Orrù, P.F.; Buonadonna, P. Product Quality and Energy Consumption Optimisation of Dyeing Fixing Process by Steaming through DOE Analysis: A Cotton Case Study. *Int. J. Manag. Decis. Mak.* **2018**, *17*, 467–487. [CrossRef]
26. Lee, S.H.; Saito, Y.; Sakai, T.; Utsunomiya, H. Microstructures and Mechanical Properties of 6061 Aluminum Alloy Processed by Accumulative Roll-Bonding. *Mater. Sci. Eng. A* **2002**, *325*, 228–235. [CrossRef]

27. Lan, X.; Xiao, Y.; Hu, B.; Yang, M.; Wang, Q.; Lu, Q.; Yang, T.; Li, K.; Wang, J.; Wang, Z.; et al. Systematic Study of Growth Behavior of β-Al9Fe2Si2 in Al Alloys with High Iron and Silicon Contents. *J. Mater. Res. Technol.* **2023**, *26*, 260–266. [CrossRef]
28. Zinong, T.; Bing, Z.; Jun, J.; Zhiqiang, L.; Jianguo, L. A Study on the Hot Roll Bonding of Aluminum Alloys. *Procedia Manuf.* **2020**, *50*, 56–62. [CrossRef]